Segment-Dependent Gene Expression Profiling of the Cartilaginous Fish Nephron Using Laser Microdissection for Functional Characterization of Nephron at Segment Levels

Authors: Horie, Takashi, Takagi, Wataru, Aburatani, Naotaka, Yamazaki, Manabu, Inokuchi, Mayu, et al.

Source: Zoological Science, 40(2) : 91-104

Published By: Zoological Society of Japan

URL: https://doi.org/10.2108/zs220092

ZOOLOGICAL SCIENCE **40**: 91–104 (2023)

Segment-dependent Gene Expression Profiling of the Cartilaginous Fish Nephron Using Laser Microdissection for Functional Characterization of Nephron at Segment Levels

Takashi Horie[1], Wataru Takagi[1], Naotaka Aburatani[1], Manabu Yamazaki[1], Mayu Inokuchi[2,3], Masaya Tachizawa[2], Kataaki Okubo[2], Ritsuko Ohtani-Kaneko[3], Kotaro Tokunaga[4], Marty Kwok-Sing Wong[1,5], and Susumu Hyodo[1]*

[1]*Laboratory of Physiology, Atmosphere and Ocean Research Institute, The University of Tokyo, Kashiwa, Chiba 277-8564, Japan*
[2]*Department of Aquatic Bioscience, Graduate School of Agricultural and Life Sciences, The University of Tokyo, Bunkyo, Tokyo 113-8657, Japan*
[3]*Department of Life Sciences, Toyo University, Oura, Gunma 374-0193, Japan*
[4]*Ibaraki Prefectural Oarai Aquarium, Oarai, Ibaraki 311-1301, Japan*
[5]*Department of Biomolecular Science, Toho University, Funabashi, Chiba 274-8510, Japan*

For adaptation to a high salinity marine environment, cartilaginous fishes have evolved a ureosmotic strategy. They have a highly elaborate "four-loop nephron" in the kidney, which is considered to be important for reabsorption of urea from the glomerular filtrate to maintain a high concentration of urea in the body. However, the function and regulation, generally, of the "four-loop nephron" are still largely unknown due to the complicated configuration of the nephron and its many subdivided segments. Laser microdissection (LMD) followed by RNA-sequencing (RNA-seq) analysis is a powerful technique to obtain segment-dependent gene expression profiles. In the present study, using the kidney of cloudy catshark, *Scyliorhinus torazame*, we tested several formaldehyde-free and formaldehyde-based fixatives to optimize the fixation methods. Fixation by 1% neutral buffered formalin for 15 min resulted in sufficient RNA and structural integrities, which allowed LMD clipping of specific nephron segments and subsequent RNA-seq analysis. RNA-seq from the LMD samples of the second-loop, the fourth-loop, and the five tubular segments in the bundle zone revealed a number of specific membrane transporter genes that can characterize each segment. Among them, we examined expressions of the Na^+-coupled cotransporters abundantly expressed in the second loop samples. Although the proximal II segment of the second loop is known for the elimination of excess solutes, the present results imply that the PII segment is also crucial for reabsorption of valuable solutes. Looking ahead to future studies, the segment-dependent gene expression profiling will be a powerful technique for unraveling the renal mechanisms and regulation in euryhaline elasmobranchs.

Key words: cartilaginous fish, kidney, laser microdissection, RNA-sequencing, membrane transporter, gene expression profiling

INTRODUCTION

The marine environment is a high salinity environment, and organisms have adapted to this environment by adopting various physiological strategies. The strategy adopted by cartilaginous fish (sharks, rays, skates, and chimaeras) is well recognized as urea-based osmoregulation (also referred to as a ureosmotic strategy) (Pang et al., 1977; Hazon et al., 2003). The ureosmotic animals maintain their plasma ions at levels approximately half of seawater (SW), while plasma osmolality is slightly hyperosmotic to the surrounding SW through active production and retention of urea. As a result, they do not suffer dehydration even in the high salinity marine environment (Anderson et al., 2007).

Multiple organs are involved in maintaining body-fluid

* Corresponding author. E-mail: hyodo@aori.u-tokyo.ac.jp
doi:10.2108/zs220092

homeostasis of cartilaginous fishes. Among these, the kidney is one of the most important organs to achieve the ureosmotic strategy. Although urea is a key osmolyte to maintain the high plasma osmolality of cartilaginous fish, this osmolyte is freely filtered by the glomerulus. Despite the potential loss, more than 90% of filtered urea is reabsorbed from the glomerular filtrate by the renal tubules (Smith, 1936; Kempton, 1953; Boylan, 1967). Therefore, renal excretion of urea accounts for less than 20% of total urea loss (Goldstein and Forster, 1971; Payan et al., 1973). Meanwhile, the pioneering works by Lacy and Reale (1985a, b) and Hentschel et al. (1993) described the highly elaborated renal nephron as follows. Each nephron begins at a renal corpuscle and forms four loops that traverse repeatedly between two distinct regions, the bundle and sinus zones, within the kidney. Beginning from Bowman's capsule, each nephron consists of the neck, proximal, intermediate, distal, and collecting tubules. The proximal, intermediate, and distal tubules are further subdivided into multiple segments with different morphological characteristics (Lacy and Reale, 1985b; Hentschel, 1987; Kakumura et al., 2015). The characteristic structure of the "four-loop nephron" is considered to be important to perform dedicated roles in each segment and contribute to its overall function, such as urea reabsorption from the glomerular filtrate (see Hyodo et al., 2014).

In order to clarify the function of elasmobranch nephrons, we have conducted mapping studies of various ion pumps, channels, and transporters in the nephron segments. For instance, a facilitative urea transporter (UT; Slc14a1/2) is expressed in the collecting tubule, the final segment of the nephron, while Na^+/K^+-ATPase (NKA) and $Na^+,K^+,2Cl^-$ cotransporter (NKCC2; Slc12a2) are co-localized in the early and late distal tubules, implying that the distal tubules could be segments for desalination (Hyodo et al., 2004; Kakumura et al., 2015; Imaseki et al., 2019; Aburatani et al., 2020, 2022). Based on these results, our group proposed a model for urea reabsorption where urea is reabsorbed in the collecting tubule through the coordinated reabsorption of water and NaCl in the first and/or the third loops in the bundle zone (Hyodo et al., 2014). Likewise, based on our findings, expressions of sulfate transporters (Slc26a1, Slc26a6) were detected in the proximal II (PII) segment, indicating that the PII segment in the sinus zone is involved in sulfate excretion (Hasegawa et al., 2016). In these investigations, expression analyses of target genes or RNA-sequencing (RNA-seq) were conducted using a portion of whole kidney. These whole tissue analyses lack the needed resolution to allow comprehensive gene expression analysis at segment levels, and thus it limits advancement in functional and regulatory studies of each nephron segment.

Laser microdissection (LMD) clips a particular cell(s) or a piece of tissue from a tissue section (Espina et al., 2006; Murray, 2007). Recently, proximal and distal tubule cells were dissected separately by laser capture microdissection and relative mRNA expression levels of segment-specific solute and water transporters were quantified in Atlantic salmon acclimated to fresh water and SW (Madsen et al., 2020). By using the LMD technique, we expect that segment-specific gene expression profiling can also be obtained in the highly elaborate cartilaginous fish nephron. In the LMD clipping, unfixed tissue sections instantly frozen are recommended to preserve RNA integrity for the subsequent gene expression analysis. However, in the case of cartilaginous fish kidney, multiple nephron segments are mixed in a small area. To identify the segment accurately, it is necessary to stain the fixed tissue briefly before conducting LMD. In general, formaldehyde is used in many fixation procedures because it preserves morphology. However, formaldehyde also cross-links nucleic acids and proteins (Park et al., 1996; Chung et al., 2008) and covalently modifies RNA, hindering the RNA extraction, reverse transcription, and quantitation (Auerbach et al., 1977; Masuda et al., 1999).

In the present study, we therefore aimed to optimize the fixation conditions and RNA extraction method, which allowed LMD clipping of a specific nephron segment for subsequent RNA-seq analysis. To confirm the segment-specific clipping by LMD, four established marker genes (sodium-glucose cotransporter 2 [*sglt2, slc5a2*], *nkcc2*, Na^+-Cl^- cotransporter [*ncc, slc12a3*], and *ut*) were used to evaluate the clipping accuracy of each segment. Immunoreactive SGLT2 is abundantly localized in the proximal I segment (the first loop) in spiny dogfish *Squalus acanthias* (Althoff et al., 2006), while *nkcc2* and *ncc* are expressed in the third and fourth loops, and the fourth loop, respectively (Kakumura et al., 2015; Imaseki et al., 2019; Aburatani et al., 2022). *ut* is almost exclusively found in the final segment (collecting tubule) in all cartilaginous fish nephrons thus far examined (Hyodo et al., 2004; Kakumura et al., 2015; Imaseki et al., 2019; Aburatani et al., 2020). Following the segment-specific gene profiling, selected co-transporter genes that were highly expressed in the PII segment (second loop of nephron) were further examined by in situ hybridization. Since the function of PII segment is less well described, our approach successfully increases the knowledge of the functions of this nephron segment de novo.

MATERIALS AND METHODS

Animals

Adult cloudy catsharks (*Scyliorhinus torazame*) were transported from Ibaraki Prefectural Oarai Aquarium to the Atmosphere and Ocean Research Institute at The University of Tokyo. They were kept in 3000 L tanks with recirculating natural SW under a constant photoperiod (light: dark; 12 h: 12 h) at 16°C. Fertilized eggs were collected from captive individuals, and eggs and hatched juveniles were maintained in 1000 L tanks under the same environmental conditions. Both adults and juveniles were fed with chopped squid or sardine to satiation twice a week. All experimental procedures were approved by the Animal Ethics Committee of the Atmosphere and Ocean Research Institute of The University of Tokyo (P19-2). The present study was carried out in compliance with the ARRIVE guidelines.

Tissue preparation for laser microdissection (LMD)

Juvenile catsharks were euthanized with 0.02% (w/v) ethyl 3-aminobenzoate methanesulfonate (Sigma-Aldrich, MO, USA), and whole kidneys were dissected out. The dissected kidneys were sliced transversely into approximately 2 mm-thick kidney blocks. Some blocks were frozen immediately in liquid N_2, and the other blocks were fixed using various protocols summarized in Table 1. The fixatives used in the present study are as follows: Methacarn (methanol: chloroform: acetic acid = 6: 3: 1) (Puchtler et al., 1970); UMFIX (methanol: polyethylene glycol 300 = 17: 3) (Vincek et al., 2003); Z7 (0.5% zinc chloride, 17.16 mM zinc trifluoroacetate, 0.05% calcium acetate in 0.1 M Tris-HCl, pH 6.4 to 6.7) (Lykidis et al.,

Table 1. Fixatives used in the present study and corresponding RNA integrity numbers.

Fixatives	Fixation condition	Fixation time	RNA integrity number (RIN)					
			Cryostat			Scraped off		
Unfixed	frozen		7	4.8	5.4	4.6	2.7	6.5
Formaldehyde-free fixatives								
Methacarn	4°C	1 hr	7	6.2	7.3	2.9	2.4	6.7
UMFIX	4°C	3 hr	3.4			7.6		
UMFIX	4°C	12 hr	6.8			8		
Z7	4°C	3 hr	8	7.5	5.6	7.7	8	8
Z7	4°C	12 hr	8	5.4	6.2	6.9	3.6	7.7
Formaldehyde-containing fixatives								
4% PFA	RT	overnight				3.3	3	
10% NBF	4°C, under negative pressure	5 min	5.8			1		
10% NBF	4°C	1 min	7.9			8		
1% NBF	4°C	1 min	7.3	8.1		7.5	7.8	
1% NBF	4°C	15 min	1.5	8.3		7.8	8.1	

The shadowed entries are RIN values less than 5.0. “Cryostat” and “Scraped off” represents the tissues following cryostat sectioning without mounting on glass slide, and the tissues scraped off from glass slides following hematoxylin staining, respectively.

2007); 4% PFA (4% paraformaldehyde in 0.1 M phosphate buffer [pH 7.4] containing 150 mM NaCl and 350 mM urea); 10% NBF (commercial 10% formalin neutral buffer solution [Wako Pure Chemical Industries, Osaka, Japan]), and 1% NBF (1% NBF in 20% sucrose).

Fixed blocks of kidney tissue were washed once in Optimal Cutting Temperature (O.C.T.) compound (Sakura Finetek Japan, Tokyo, Japan), and embedded in new O.C.T. compound. All of the embedded blocks were stored at –80°C until sectioning. Frozen blocks were cut at 10 μm using a cryostat maintained at –20°C and consecutive sections were mounted alternatively onto MembraneSlide NF 1.0 PEN (Carl Zeiss Micro Imaging, Jena, Germany) for LMD use or onto MAS-GP-coated glass slides (Matsunami Glass, Osaka, Japan) for reference. This allows a reference histological image of the adjacent section for each LMD-slide. The slides were dried in a cryostat for at least 2 min, followed by fixation in 70% ethanol for 5 min, and then washed with distilled water (DW) for 1 min twice.

Sections on the LMD-slides were stained with Mayer’s hematoxylin solution (Wako Pure Chemical Industries) for 1 min, and hematoxylin coloration was enhanced by incubation in DW at 40°C for 1 min. Sections were washed with 70% ethanol for 5 min, dehydrated through graded ethanol of 70%, 95%, and 100% (1 min each), and rapidly dried with a hair dryer. After spraying Liquid Cover Glass (Carl Zeiss Micro Imaging) on the sections, the slides were placed in 50 ml tubes and stored at –80°C until use. All of the staining procedures were performed on ice, except for the coloration enhancement step after hematoxylin staining.

Sections on the reference-slides were stained with the Periodic acid Schiff (PAS) method. Sections were stained with 0.5% Periodic acid solution (Wako Pure Chemical Industries) for 5 min, washed with tap water for 3 min once and then with DW for 5 min three times. Sections were then incubated with Schiff’s reagent (Wako Pure Chemical Industries) for 15 min. After rinsing with sulfurous acid solution (10% sodium bisulfite: 1 N HCl: DW = 6: 5: 100) for 3 min three times, the sections were washed with DW for 5 min three times, and then counterstained with Mayer’s hematoxylin solution for 3 min. To promote hematoxylin coloration, the sections were washed with running tap water for 15 min. The sections were washed with DW for 3 min, and then dehydrated through the graded ethanol series, cleared in xylene, and mounted with Permount (Thermo Fisher Scientific, Waltham, MA, USA).

RNA extraction and evaluation of the quality of RNA

Total RNA was extracted from two sections (10 μm each) directly from the cryostat, or six scraped-off sections after hematoxylin staining with a FastGene RNA Basic Kit according to the manufacturer’s protocol (Nippon Genetics, Tokyo, Japan). RNA quality was assessed by microcapillary electrophoresis with the RNA 6000 Pico LabChip kit (Agilent Biotechnologies, Tokyo, Japan) and the Agilent 2100 bioanalyzer (Agilent Biotechnologies), which assigns an RNA integrity number (RIN) to each RNA electropherogram. This number ranges from 1 (completely degraded RNA sample) to 10 (intact RNA sample) (Schroeder et al., 2006).

LMD and Quartz-Seq

The PALM MicroBeam System (Carl Zeiss Micro Imaging) at Toyo University Itakura Campus was used to excise the selected tissue areas on the LMD slides. The selected tissue areas were determined according to the morphological identification in the reference slides that contain the adjacent sections after PAS-staining. The frozen LMD slides were transferred to the laser microscope (PALM) immediately after being brought to room temperature. The narrow beam ultraviolet laser cut out the areas of interest from surrounding tissue, and the laser was then used to catapult the microdissected areas into collecting caps of AdhesiveCap 500 clear tubes (Carl Zeiss Micro Imaging). In the present study, the bundle zone (“Bundle”; a mixture of the first loop, third loop and final segment), the PII segment of the second loop (“2nd”) and the late distal tubule (LDT) of the fourth loop (“4th”) were excised from 12 cryosections, and stored at –80°C until being extracted.

Total RNA from LMD-excised renal segments was extracted using an RNeasy® Micro Kit (Qiagen, Tokyo, Japan) according to the manufacturer’s protocol. Total RNA concentration was measured using the QuantiFluor RNA System (Promega, Madison, WI, USA). Quartz-Seq (Sasagawa et al., 2013) was performed to amplify cDNA from the low-yield total RNA. Firstly, total RNA was added to Quartz-RT primer (5′-TATAGAATTCGCGGCCGCTCGCG ATAATACGACTCACTATAGGGCG$(T)_{24}$-3′), dNTPs (Thermo Fisher Scientific), and RNasin Plus (Promega) at 12 μl solution and the mixtures were treated at 70°C for 90 s and at 35°C for 15 s to prime the RNA with RT primers. Then, SuperScript III (Thermo Fisher Scientific) master mix was added to a final volume of 20 μl and the reverse transcription reaction was performed at 35°C for 5 min and 45°C for 20 min, followed by a 10 min treatment at 70°C to inactivate the reverse transcriptase. The resulting first-strand cDNA was purified with Agencourt AMPure XP beads (Beckman Coulter, Brea, CA, USA) and treated with Exonuclease I (Takara Bio, Shiga, Japan) at 37°C for 30 min to digest the excess RT primers. Exonuclease I was inactivated by incubation at 80°C for 20 min. After that, the Poly-A tailing reaction was performed by adding reaction mixture containing dATP (Thermo Fisher Scientific), RNase H (Thermo Fisher Scientific), and Terminal Transferase (Roche Applied Science, Mannheim, Germany). A reaction mix containing Quartz-Tagging primer (5′-TATAGAATTCGCGGCCGCTCGCGA$(T)_{24}$-3′) and MightyAmp DNA polymerase (Takara Bio) was prepared on ice and added to the cDNA templates. The double-stranded DNA synthesis reaction was carried out at 98°C for 2 min 10 sec, 40°C for 1 min, and 68°C for 5 min. After the reaction, the solution was placed on ice to stop the reaction. cDNA was then amplified in a 107 μl reaction system with Quartz-PCR primer (5′-NH_2-GTATAGAATTCGCGGCCGCTCGCGAT-3′). cDNA amplification was carried out in 18 amplification cycles at 98°C for 10 s, 65°C for

15 s, and 68°C for 5 min. To verify the quality of the amplified cDNA, 4 μl of the reaction product was electrophoresed on a 1.5% agarose gel. A successful cDNA amplification resulted in a smear of DNA at various lengths. Subsequently, the product was purified using MinElute PCR Purification Kit (Qiagen) and the cDNA concentration was measured using Qubit 4 (Thermo Fisher Scientific) and the Qubit dsDNA HS Assay Kit (Thermo Fisher Scientific) and Qubit Assay Tubes (Thermo Fisher Scientific).

RNA-seq analysis

RNA-seq library preparation, sequencing, mapping, and gene expression analysis were performed by DNAFORM (Yokohama, Kanagawa, Japan).

Double-stranded cDNA libraries (RNA-seq libraries) were prepared from the cDNA amplified by Quartz-Seq using the SMART-Seq Stranded Kit (Takara Bio) according to the manufacturer's instruction. The "Bundle", the "2nd", and the "4th" samples of catshark kidney were analyzed (n = 3). RNA-seq libraries were sequenced using 150 bp paired end reads on a NextSeq 500 instrument (Illumina, San Diego, CA, USA). Qualified reads were mapped to the catshark Genome assembly: Storazame_v1.0 using STAR (version 2.7.2) (Dobin et al., 2013). Reads on annotated genes were counted using featureCounts (version 1.6.1) (Liao et al., 2014). Transcripts per million (TPM) values were calculated from the mapped reads and normalized to total counts of transcript, and the TPM values for each segment were arranged in a descending order. The expression levels among the three segments (Bundle, 2nd, and 4th) were then statistically analyzed. All of the coding nucleotide sequences predicted on the catshark genome were subjected to NCBI blastx (Expect threshold: 0.05) against the non-redundant protein sequences to identify the putative proteins. The gene names, protein names, and Gene Ontology (GO) terms corresponding to all of the identified proteins were acquired through Uniprot database. The genes containing GO terms of molecular function "transporter activity" and cellular component "plasma membrane" were then short-listed. The raw sequenced reads were deposited in the DNA Data Bank of Japan (DDBJ) under the accession numbers DRR413293–DRR413301.

cDNA cloning

Complementary DNA cloning was performed as previously described in detail (Takagi et al., 2017) using frozen kidney of juvenile catshark. Total RNA was extracted using ISOGEN (Nippon Gene, Toyama, Japan). DNase-treated total RNA (1 μg) was reverse-transcribed into cDNA using a High Capacity cDNA Reverse Transcription Kit (Thermo Fisher Scientific), following the manufacturer's instructions. Putative nucleotide sequences of mRNAs encoding catshark SGLT2, NKCC2, NCC, UT, Slc1a3, Slc5a8, Slc5a11, Slc13a3, and β-actin were obtained by BLAST search on catshark transcriptome database Squalomix (https://transcriptome.riken.jp/squalomix/) (Hara et al., 2018). Partial cDNA fragments, which were amplified with Kapa Taq Extra DNA polymerase (Kapa Biosystems, Boston, MA, USA) and gene-specific primer sets (see Supplementary Table S1), were ligated into pGEM-T Easy plasmid vector (Promega). The nucleotide sequences were determined using a DNA sequencer (ABI PRISM 3130, Life Technologies, Carlsbad, CA, USA). The sequence data were deposited in the DDBJ under the accession numbers LC739024 (*ncc*), LC739025 (*sglt2*), LC739026 (*nkcc2*), LC739027 (*ut*), LC739028 (*slc1a3*), LC739029 (*slc5a8*), LC739030 (*slc5a11*), and LC739031 (*slc13a3*).

In situ hybridization

Kidneys of adult female catsharks fixed in Bouin's solution without acetic acid were embedded in Paraplast (McCormick Scientific, Richmond, IL, USA). Serial sections were prepared at 7 μm and mounted onto MAS-coated slides (Matsunami Glass). The cloned cDNAs were amplified from the plasmids with Primestar GXL DNA polymerase (Takara Bio) using M13 forward and reverse primers. The PCR products were subsequently purified using Wizard SV Gel and PCR Clean-up System (Promega) and used to synthesize digoxigenin (DIG)-labeled antisense and sense cRNA probes with a DIG RNA labeling kit (Roche Applied Science), following the manufacturer's protocols. Hybridization and washing were conducted using a previously described protocol (Aburatani et al., 2022). Stained sections were counterstained with Kernechtrot Stain Solution (MUTO PURE CHEMICALS, Tokyo, Japan) and mounted using Permount (Thermo Fisher Scientific) (*sglt2*, *nkcc2*, *ncc*, and *ut*), or mounted using CC/Mount (Diagnostic BioSystems, Pleasanton, CA, USA) without counterstaning for weakly stained sections (*slc1a3*, *slc5a8*, *slc5a11*, and *slc13a3*).

Quantitative real-time PCR (qPCR)

The gene expression levels were measured by qPCR using 7900HT Fast Real Time PCR System (Applied Biosystems, Forster city, CA, USA) with a KAPA SYBR FAST qPCR Kit (Kapa Biosystems) and gene-specific primer sets (see Supplementary Table S1). The cloned plasmids containing the target sequences were serially diluted as standard templates for quantification. The expression levels of β-actin mRNA were used as internal control.

Statistical analysis

Values are presented as means ± S.E.M. The qPCR results were analyzed by one-way ANOVA followed by Tukey's multiple comparison test or Kruskal-Wallis test followed by Dunn's multiple comparison test. The TPM values among the three segments (Bundle, 2nd, and 4th) were analyzed by one-way ANOVA followed by Tukey's multiple comparison test. P values < 0.05 were considered as statistically significant. All analyses were performed using Prism Ver. 9 for Windows (GraphPad, San Diego, CA, USA).

RESULTS

Evaluation of tissue preparation methods

For successful LMD dissection and subsequent RNA-seq, an optimal fixation method that provides substantial histological resolution and RNA integrity is required. To avoid possible cross-linking damage to RNA integrity by formaldehyde, several formaldehyde-free fixatives, Methacarn, UMFIX, and Z7, were examined (Table 1). The RNA quality was assessed by the RNA integrity number (RIN) in an RNA electropherogram. For each fixation method, RNA samples were prepared from 1) the tissues following cryostat sectioning without mounting on glass slides ("Cryostat") and 2) the tissues scraped off from glass slides following hematoxylin staining ("Scraped off"). The RNA samples prepared from the unfixed tissues had RIN values between 5.73 ± 0.66 ("Cryostat") and 4.60 ± 1.10 ("Scraped off"). Most RNA samples from fixed tissues with formaldehyde-free fixatives had RIN values higher than 5, but some samples from the Methacarn-fixed for 1 h, UMFIX-fixed for 3 h, and Z7 for 12h had RIN values lower than 5 (Table 1). On the other hand, RNA samples prepared from the formalin-fixed paraffin-embedded (4% PFA overnight) tissues had RIN values less than 3.5, which was considerably lower than those of formaldehyde-free fixatives.

Figure 1A shows the transverse section of the formaldehyde-fixed kidney of adult catshark. The kidney consists of the sinus zone and the bundle zone, with single nephrons traversing repeatedly between the two zones (see Fig. 1D). The sinus zone is filled with the second and the fourth loops (Fig. 1B), while five tubular segments (the descending and

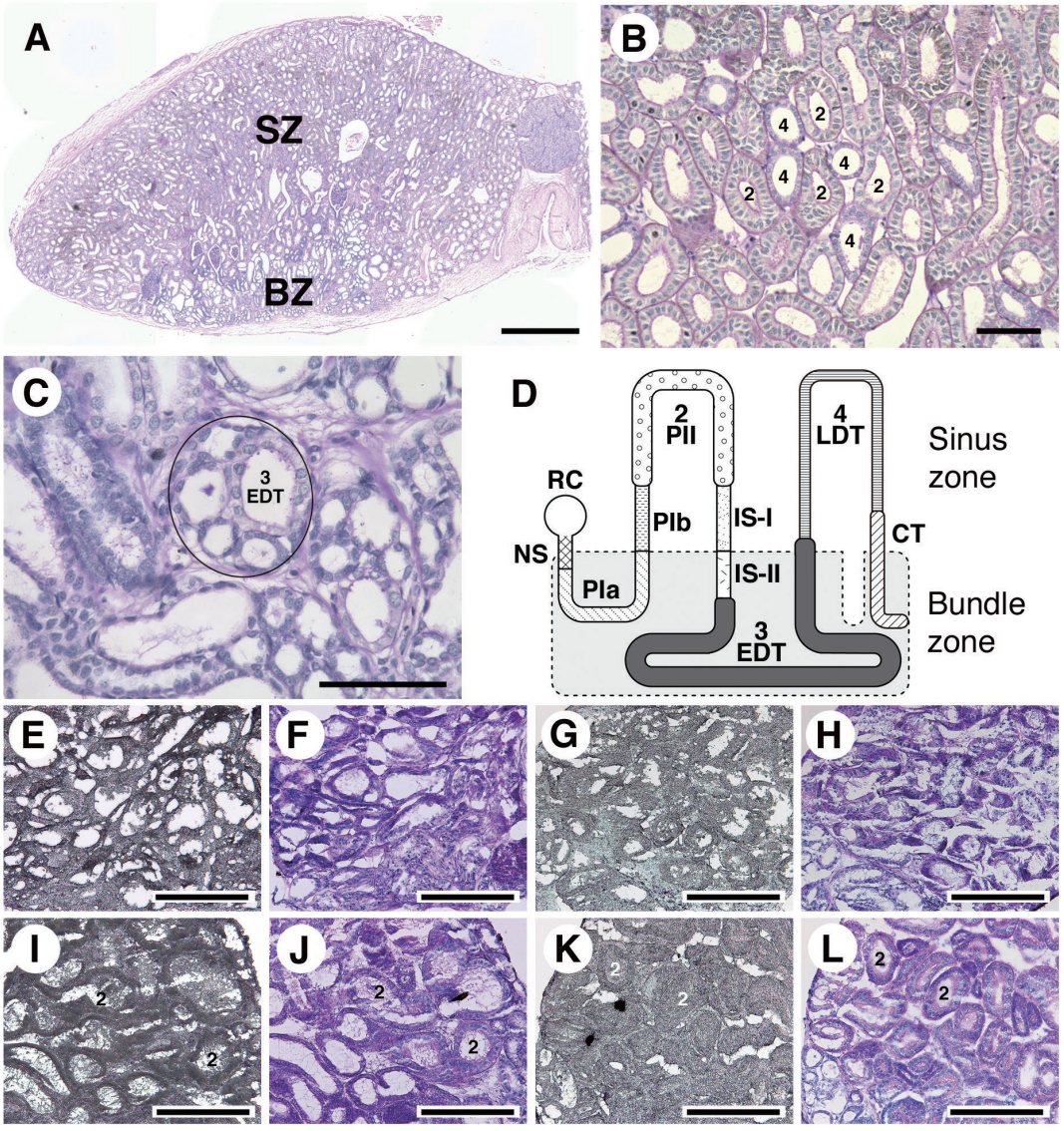

Fig. 1. Anatomical features of the cartilaginous fish kidney and histological preservation by the formaldehyde-free and formaldehyde-based fixatives for LMD. **(A)** Transverse section of the formaldehyde-fixed adult catshark kidney stained with PAS. SZ, sinus zone; BZ, bundle zone. **(B)** Magnified image of the sinus zone. The number labels 2 and 4 mark the PII segment and the LDT, respectively. Note that, in the case of PII segment, the brush border of the apical surface is stained with PAS. **(C)** Magnified view of the bundle zone. The circle represents five tubular segments of a single nephron. **(D)** Schematic illustration of cartilaginous fish nephron. CT, collecting tubule; EDT, early distal tubule; IS, intermediate segment; LDT, late distal tubule; NS, neck segment; PI and PII, proximal segment I and II, respectively; RC, renal corpuscle. **(E–L)** Histological images of catshark kidney for LMD (hematoxylin-stained **[E, G, I, K]**) and reference (PAS-stained **[F, H, J, L]**) slides. Tissues were fixed with UNFIX for 12 h **(E, F)**, Z7 for 12 h **(G, H)**, 10% NBF for 1 min **(I, J)**, or 1% NBF for 15 min **(K, L)**. The number label 2 represents the PII segment of second loop. Scale bars: 1 mm **(A)**, 100 μm **(B, C)**, 300 μm **(E–L)**.

ascending segments of the first and third loops and the collecting tubule) are aggregated in the bundle zone. The five bundle segments were closely wrapped by a sac-like peritubular sheath (circled in Fig. 1C). Figure 1E, G represent the sinus zone of UMFIX- and Z7-fixed kidney samples, respectively, and histological preservation by the formaldehyde-free fixatives was too low for identifying specific segments for the subsequent LMD. In addition, during the preparation of the adjacent sections for PAS staining, we noticed that histological structures were easily distorted in the formaldehyde-free fixed sections, and thus confident identification of specific tubular segments on the reference slides was not possible (Fig. 1F, H).

The above results suggest that the formaldehyde-free fixatives examined so far are not suitable for excising specific nephron segments using LMD. Therefore, the use of formaldehyde-based fixatives was examined (Table 1). The low RIN score in the 4% PFA overnight samples might be due to excessive cross-linking and modification of nucleic acids by formaldehyde, and possible damage to nucleic acids by formic acid produced by the oxidation of formaldehyde. Therefore, we next examined various fixation conditions for frozen tissues using a commercial 10% neutral buffered formalin (NBF; approximately 3.7% paraformal-

dehyde) solution. Four conditions were examined: 1) 10% NBF for 5 min under negative pressure, 2) 10% NBF for 1 min, 3) 1% NBF in 20% sucrose for 1 min, and 4) 1% NBF in 20% sucrose for 15 min (Table 1). Fixation in 10% NBF under negative pressure is considered to facilitate formaldehyde penetration into the tissues, thereby minimizing the exposure time to formaldehyde. However, the RIN scores were 5.80 and 1.00, indicating that the negative pressure protocol was not compatible with RNA extraction. On the other hand, the reduced fixation time for 1 min in 10% NBF achieved high RIN scores of 7.90 and 8.00. Furthermore, a low concentration of NBF at 1% for 1 min or 15 min also improved RIN score to over 7.0 except for one sample fixed in 1% NBF for 15 min (Table 1).

Cryostat sections with formaldehyde-based fixatives improved histological preservation compared to those with formaldehyde-free fixatives (Fig. 1I, K). When adjacent sections were stained with PAS, the proximal segment of the second loop and the distal segment of the fourth loop were clearly distinguishable by the presence and absence, respectively, of brush border on the apical surface of lumen (Fig. 1J, L). Although both fixation times of 1 min and 15 min resulted in satisfactory RIN values, the longer fixation time reduced the hastiness of the procedures and thus produced a more consistent fixation condition. Collectively, fixation in a low-concentration formaldehyde (1% NBF) for 15 min maintains a reasonable tissue morphology and RNA quality, and thus allows LMD clipping of specific renal tubules for subsequent RNA-seq.

Evaluation of segment specificity of LMD samples

Four membrane transporter genes were selected as markers as they are specifically and abundantly expressed in particular segments of the nephron according to previous studies. Segment-specific expressions of these marker genes were confirmed in the catshark kidney (Fig. 2). Signals for *sglt2* mRNA were detected in the bundle zone, but not in the sinus zone (Fig. 2A–C). In the bundle zone, *sglt2* mRNA signals were observed only in a single nephron segment (open arrowheads in Fig. 2B). Observation using serial

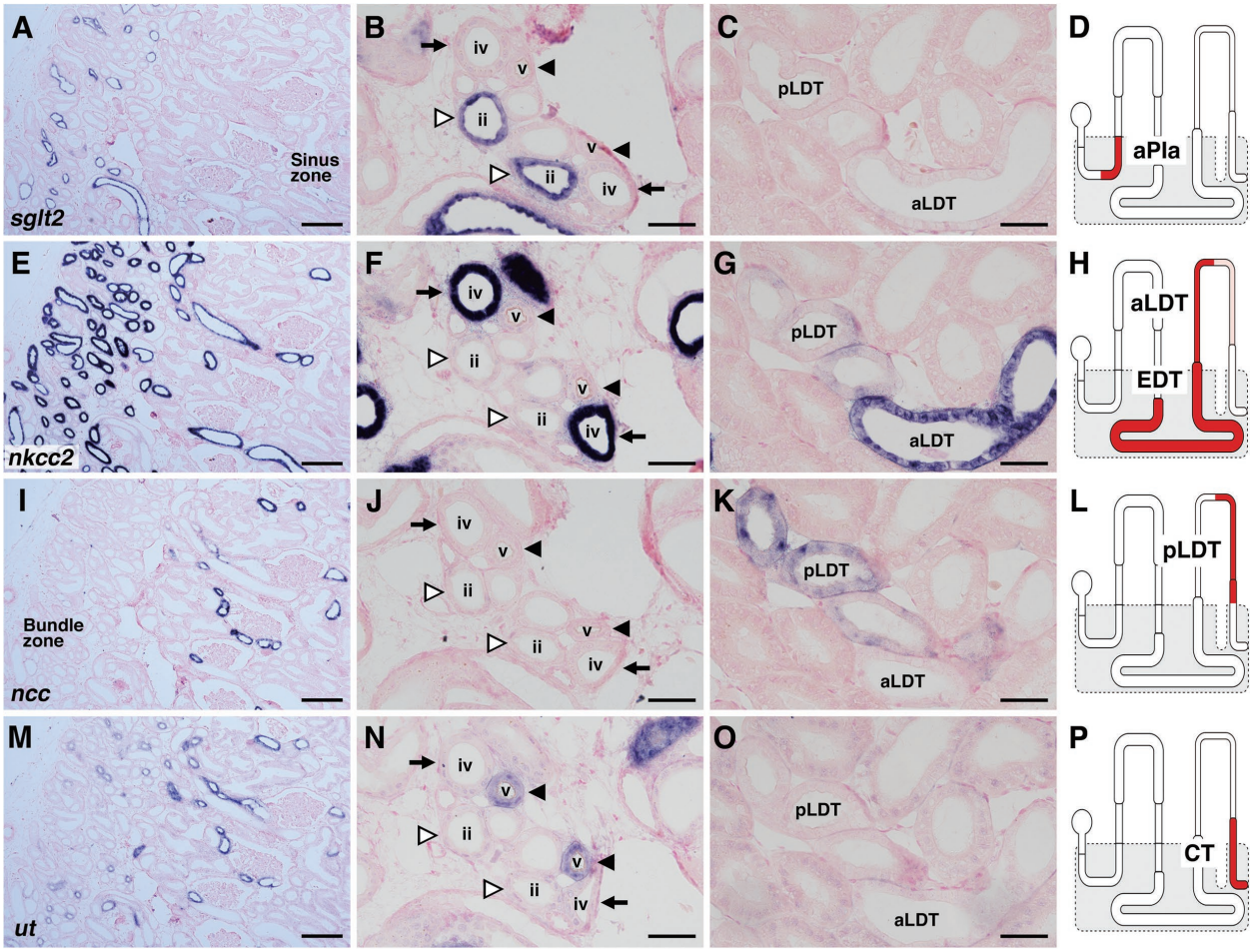

Fig. 2. Expression of the marker genes used in the present study. **(A–D)** Na^+-coupled glucose transporter (*sglt2* mRNA), **(E–H)** Na^+,K^+,$2Cl^-$ cotransporter (*nkcc2* mRNA), **(I–L)** Na^+,Cl^- cotransporter (*ncc* mRNA), **(M–P)** urea transporter (*ut* mRNA). **(A, E, I, M)** Low magnification of catshark kidney showing both the bundle and sinus zones. Magnified views of the bundle zone **(B, F, J, N)** and the sinus zone **(C, G, K, O)**. The marks represent the following: open arrowheads, the ascending part of the PIa segment ("ii" in the tubules); arrows, the EDT of the third loop ("iv" in the tubules); arrowheads, the collecting tubule ("v" in the tubules); aLDT and pLDT, anterior and posterior LDT, respectively. **(D, H, L, P)** Schematic images representing localization of *sglt2* **(D)**, *nkcc2* **(H)**, *ncc* **(L)**, and *ut* **(P)** mRNAs that are shown in red color. aPIa, ascending part of PIa segment. Scale bars: 200 μm **(A, E, I, M)** and 50 μm **(B, C, F, G, J, K, N, O)**.

sections revealed that the *sglt2* mRNA-expressing tubule is the ascending (posterior) limb of the PIa segment (Fig. 2D). On the other hand, *nkcc2* mRNA signals were found both in the bundle and sinus zones (Figs. 2E–G). In the bundle zone, intense *nkcc2* mRNA signals were detected in tubules comprised of the largest columnar cells, indicating that the early distal tubule (EDT; filled arrows) of the third loop expresses *nkcc2* mRNA (Fig. 2F, H). In the sinus zone, *nkcc2* mRNA was detected in tubules comprised of small and thin squamous cells, indicating that *nkcc2* mRNA is expressed in the fourth loop (the late distal tubule; LDT) (Fig. 2G, H). The *ncc* mRNA signals were observed in the LDT and the transitional region between LDT and CT (Fig. 2I, K). In the sinus zone, however, the posterior half of LDT was intensely stained by *ncc* mRNA signals, which was different from the anterior half of the LDT that was intensely stained by *nkcc2* mRNA (Fig. 2G, H, K, L). The *ut* mRNA signals were found in the tubules in bundle zone (Fig. 2M), and the *ut* mRNA positive segment (filled arrowheads in Fig. 2N) did not overlap with segments expressing *sglt2* (open arrowheads) or *nkcc2* (filled arrows) mRNAs, indicating that the *ut* mRNA-positive segment is the collecting tubule and preceding transitional region between LDT and CT (Fig. 2P). These results confirmed that the four marker genes are effective for evaluating segment specificity of LMD samples.

In the present LMD study, three regions of catshark nephron were excised: 1) five tubular segments wrapped by the peritubular sheath in the bundle zone ("Bundle", the descending and ascending segments of the first and third loops, and the collecting tubule), 2) the PII segment of the second loop ("2nd"), and 3) the LDT of the fourth loop ("4th"). Although no significant difference was observed in marker gene expressions among the LMD samples due to the large variations in observed data, qPCR analysis revealed that the expression of four marker genes in the LMD samples corresponded to the local abundance of mRNA shown by the results of in situ hybridization (Fig. 3). Expressions of *sglt2*, *nkcc2*, and *ut* were observed in the "Bundle" samples, in which the first loop, third loop, and collecting tubule were included. Expression of *nkcc2* mRNA was also found in the "4th" samples. Expression of *ncc* mRNA was detected in the "4th" samples, while none of the four genes had high expression in the "2nd" samples. These results further demonstrated that contamination of other segments is negligible for the obtained LMD samples.

Expression profiles of membrane transporter mRNAs in the LMD samples

Segment-dependent mRNA expression profiles were examined using three individuals. In the present study, we focused on membrane transport proteins, including the solute carrier (Slc) family, for deducing the reabsorbing and/or secreting functions of each nephron segment. By searching GO terms as described in the Methods section, we shortlisted the top 30 highly expressed membrane transporter genes in each LMD segment (Tables 2 to 4), and we statistically analyzed their expression levels among the three LMD segments. As a result, five, 13, and four genes were found to be significantly expressed in the "Bundle", "2nd", and "4th" segments, respectively, which characterize the functions of those segments (Tables 2 to 4).

Many segment-dependent genes were detected in the second loop samples, but generally these have not been investigated yet in the elasmobranch kidneys. Therefore, we selected four genes (*slc13a3*, *slc5a8*, *slc5a11*, and *slc1a3*) and further investigated their localization by in situ hybridization (Fig. 4). *slc13a3* has the highest TPM values among Slc family genes in the second loop, and its expression was intensely detected in the sinus zone (Fig. 4A). The *slc13a3*-positive segments were relatively large and did not express *nkcc2* and *ncc* mRNAs (Fig. 4P), indicating that *slc13a3* gene expression is specific to the PII segment of second loop. The intense signals observed in the second loop by in situ hybridization were consistent with the results of RNA-seq, where the TPM value of *slc13a3* mRNA was significantly higher in the "2nd" sample than that in the "4th" and "Bundle" samples.

Two genes encoding SLC5 members (*slc5a8* and *slc5a11*) were listed as genes abundantly expressed in the second loop based on RNA-seq. However, the localization

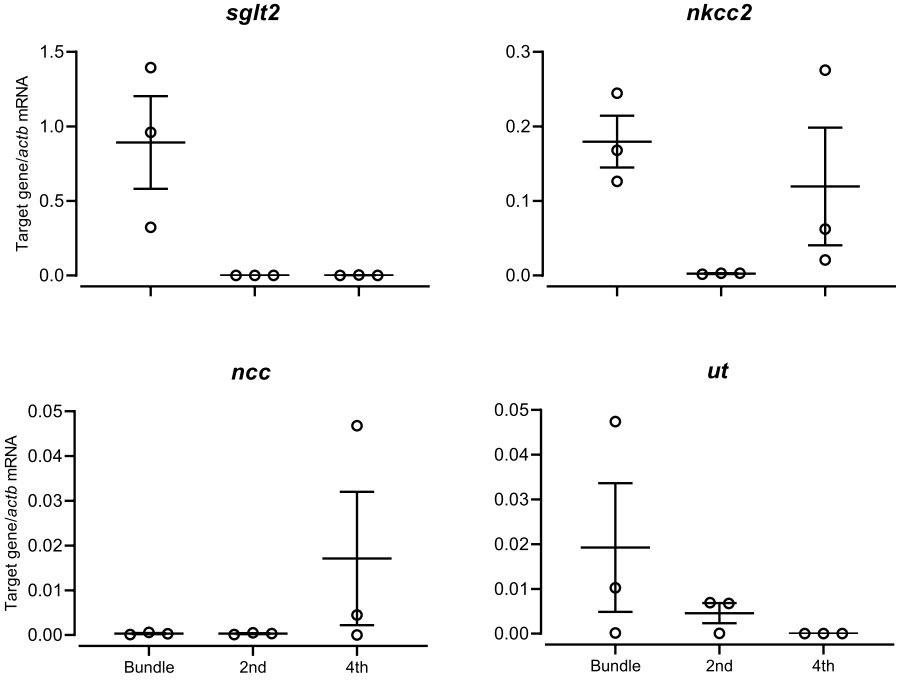

Fig. 3. Expression of the marker genes in the LMD samples for "Bundle" (five tubular segments in the bundle zone), "2nd" (the PII segment of second loop), and "4th" (the LDT of fourth loop). Data are presented as means ± S.E.M. with each sample value as an open circle (n = 3). No significant differences were observed in expressions of the marker genes among the LMD samples due to the large variations.

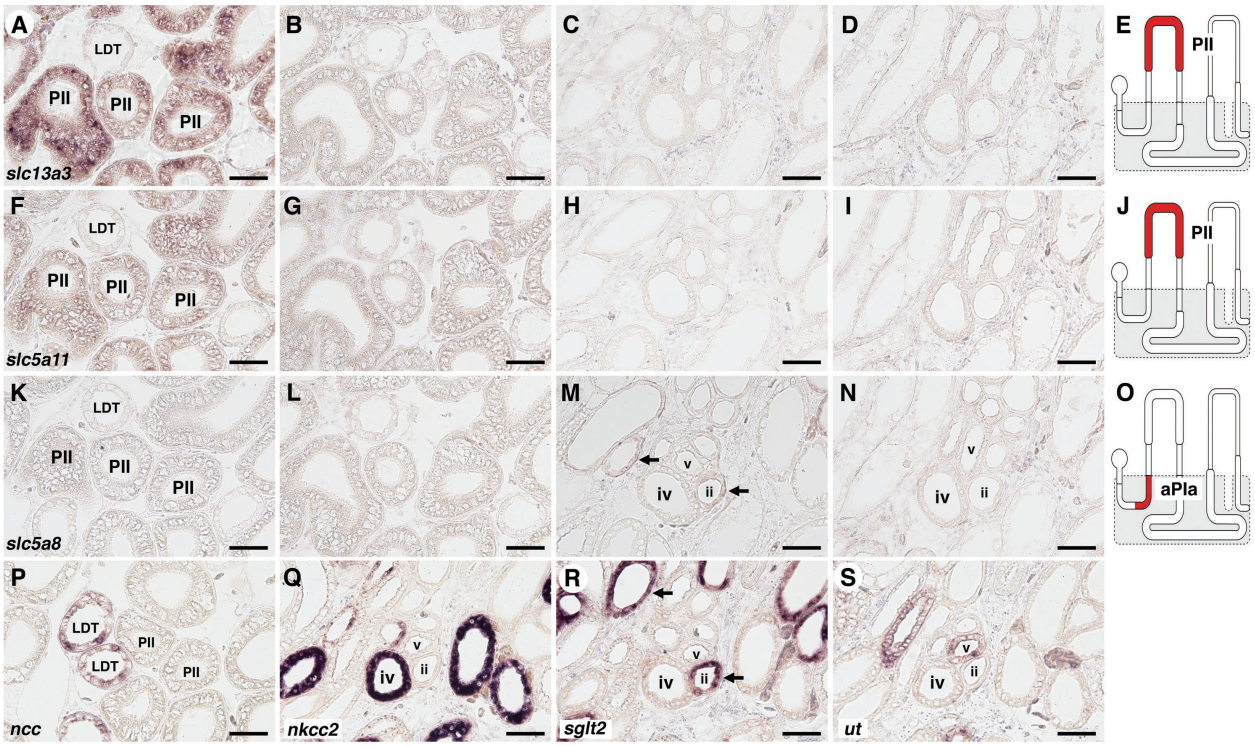

Fig. 4. Expression of *slc13a3* **(A–E)**, *slc5a11* **(F–J)** and *slc5a8* **(K–O)** mRNAs in the sinus zone **(A, B, F, G, K, L)** and the bundle zone **(C, D, H, I, M, N)** of catshark kidney. Sections were hybridized with antisense **(A, C, F, H, K, M)** or sense **(B, D, G, I, L, N)** probes. **(P–S)** Adjacent sections were stained with *ncc* (**[P]** sinus zone), *nkcc2* (**[Q]** bundle zone), *sglt2* (**[R]** bundle zone), or *ut* (**[S]** bundle zone) mRNA. The labels ii, iv, and v mark the ascending part of PIa segment, the EDT, and the collecting tubule, respectively. Both *slc13a3* and *slc5a11* mRNA signals were localized in the PII segment of the second loop **(A, F)**, while the weak mRNA signals of *slc5a8* were found in the ascending part of PIa segment (arrows in **[**M**]**), where mRNA signals of *sglt2* were co-localized (arrows in **[**R**]**). Schematic images represent localization of *slc13a3* **(E)**, *slc5a11* **(J)**, and *slc5a8* **(O)** mRNAs that are shown in red color. Scale bars, 50 μm.

patterns of *slc5a8* and *slc5a11* mRNAs in the nephron were different. The *slc5a11* mRNA signals were found only in the sinus zone (Fig. 4F). The *slc5a11*-positive tubules were the same tubules expressing *slc13a3* mRNA, although the signal intensity of *slc5a11* mRNA was much lower than that of *slc13a3* mRNA. Meanwhile, *slc5a8* mRNA signals were faintly detected in one segment within the bundle zone (arrows in Fig. 4M). The *slc5a8* mRNA-positive segment co-expressed *sglt2* mRNA (Fig. 4R) but was negative for *nkcc2* (Fig. 4Q) and *ut* (Fig. 4S) mRNAs, suggesting that *slc5a8* is expressed in the ascending part of the PIa segment of the first loop.

Although *slc1a3* mRNA was listed as a gene characteristic of the second loop, expression levels were too low to be detected by in situ hybridization. In all in situ hybridization experiments, negative control slides using sense cRNA probes resulted in no signals (Fig. 4B, D, G, I, L, N).

DISCUSSION

The cartilaginous fish nephron forms four loops that traverse repeatedly between the bundle and sinus zones. The single nephron is composed of over 10 morphologically distinct segments (Lacy and Reale, 1985b; Hentschel, 1987; Kakumura et al., 2015), and those multiple segments most likely have separate secretory and/or reabsorption functions (Hyodo et al., 2014; Hasegawa et al., 2016). However, due to technical limitations, comprehensive gene expression analyses have been conducted only using whole kidney (or a portion of whole kidney) homogenates, which has limited the search for segment-dependent gene expression that can characterize each segment. This study is the first to apply the LMD technique to analyze gene expression in the cartilaginous fish nephron, and we successfully obtained gene expression profiles that characterized three segments of the catshark nephron.

Successful clipping and gene expression profiling in each segment requires that both RNA integrity and histological preservation be relatively high. Since formaldehyde-based fixatives form cross-linkages between mRNAs and surrounding proteins, RNA integrity is often higher when the tissue is treated with formaldehyde-free fixatives. Indeed, our results showed that alcohol-based and zinc-based fixatives such as Methacarn, UMFIX, and T7 maintained high nucleic acid qualities (Table 1). However, the histological preservation by these fixatives was too low to provide essential guidance for clipping of specific nephron segments by LMD. Therefore, we tested several formaldehyde-based fixatives with modifications of fixation strength and time. Although an initial trial with 10% NBF for 5 min under negative pressure resulted in low RIN score (less than 6.0), reduction of fixation time without negative pressure or reduction of fixative concentration to 1% NBF improved the RIN scores (higher than 7.0). For RNA-seq analysis, RIN scores higher than four (Romero et al., 2014) or five (Fleige and

Table 2. List of top 30 highly expressed membrane transporter genes in the "Bundle" samples.

	GeneID	TPM									Average ± SEM			Accession	Gene name
		B_1	B_2	B_3	2nd_1	2nd_2	2nd_3	4th_1	4th_2	4th_3	Bundle	2nd	4th		
1	22033	1953.1	4293.3	1895.5	25.0	26.6	11.4	1046.1	419.1	2418.8	2714.0 ± 789.8[a]	21.0 ± 4.8[b]	1294.6 ± 590.5[ab]	P55014	Slc12a1 Nkcc2
2	11021	464.8	925.8	901.8	0.2	0.7	1.2	0.0	0.0	3.2	764.1 ± 149.8[a]	0.7 ± 0.3[b]	1.1 ± 1.1[b]	Q923I7	Slc5a2 Sglt2
3	21706	166.9	202.8	690.5	47.7	51.7	93.8	215.9	144.3	250.8	353.4 ± 168.9	64.4 ± 14.7	203.6 ± 31.3	O00299	CLIC1 G6 NCC27
4	21677	346.2	424.5	246.2	31.3	27.7	25.2	54.0	40.7	12.1	339.0 ± 51.6[a]	28.0 ± 1.8[b]	35.6 ± 12.3[b]	P07355	ANXA2 ANX2 ANX2L4 CAL1H LPC2D
5	16009	205.7	628.2	169.6	2.0	1.9	1.7	94.5	16.1	538.7	334.5 ± 147.2	1.9 ± 0.1	216.4 ± 162.7	P55016	Slc12a1 Nkcc2
6	16487	139.1	213.9	242.3	1.3	2.4	3.8	23.0	12.3	1.6	198.4 ± 30.8[a]	2.5 ± 0.7[b]	12.3 ± 6.2[b]	F1QZE9	tmc2b si:229d2.2
7	21113	187.3	307.8	92.3	193.7	377.8	153.8	238.8	117.6	237.0	195.8 ± 62.4	241.8 ± 69.0	197.8 ± 40.1	Q5ZJ06	MAGT1 RCJMB04_22a7
8	1172	56.9	300.3	7.1	23.2	40.3	70.4	0.1	0.1	25.1	121.4 ± 90.6	44.6 ± 13.8	8.4 ± 8.3	Q28614	SLC14A2 UT2
9	8888	66.3	210.2	45.4	25.8	62.6	56.3	67.6	78.0	88.0	107.3 ± 51.8	48.2 ± 11.4	77.9 ± 5.9	Q8N8Q9	NIPA2
10	8312	71.9	132.1	55.1	1.3	0.9	2.3	159.5	59.6	859.6	86.4 ± 23.4	1.5 ± 0.4	359.6 ± 251.7	Q9W701	clcnkb
11	13947	29.8	125.7	37.8	3.5	2.3	22.2	0.1	0.0	1.9	64.4 ± 30.7	9.3 ± 6.4	0.7 ± 0.6	Q2A865	Slc6a19 B0at1
12	8550	46.7	121.6	21.9	63.9	110.5	157.0	71.7	42.1	110.7	63.4 ± 30.0	110.4 ± 26.9	74.8 ± 19.9	Q9NRA2	SLC17A5
13	6217	41.7	77.2	64.7	15.9	7.0	73.5	85.2	63.0	23.8	61.2 ± 10.4	32.1 ± 20.8	57.3 ± 18.0	A8WHP3	slc5a9 si:dkey-7o6.5
14	15730	76.5	55.0	47.0	255.3	247.9	191.0	71.8	12.5	29.5	59.5 ± 8.8[a]	231.4 ± 20.3[b]	37.9 ± 17.6[a]	A1L2R7	tmem120a
15	26142	46.7	34.1	82.5	2.3	4.3	12.0	12.9	7.0	18.6	54.4 ± 14.5[a]	6.2 ± 2.9[b]	12.9 ± 3.3[b]	Q6BBL6	CLDN4
16	8632	53.3	80.3	17.6	112.3	158.8	90.0	16.4	26.0	43.6	50.4 ± 18.2[ab]	120.3 ± 20.3[a]	28.7 ± 7.9[b]	P82251	SLC7A9 BAT1
17	18278	43.9	44.0	63.0	22.1	23.5	45.7	41.0	32.3	45.2	50.3 ± 6.3	30.4 ± 7.6	39.5 ± 3.8	Q5R826	TMEM63A
18	7638	34.6	85.6	29.0	31.4	54.2	107.6	41.9	28.6	93.8	49.7 ± 18.0	64.4 ± 22.6	54.8 ± 19.9	P28288	ABCD3 PMP70 PXMP1
19	15955	42.5	84.6	21.8	0.1	3.9	2.5	165.6	269.2	520.9	49.6 ± 18.5[a]	2.2 ± 1.1[a]	318.6 ± 105.5[b]	O14764	GABRD
20	18634	42.1	52.3	52.8	51.5	28.9	37.2	3.1	13.7	0.0	49.0 ± 3.5[a]	39.2 ± 6.6[a]	5.6 ± 4.1[b]	Q90YM4	slc51b ostb
21	14778	25.6	66.9	37.5	18.6	37.9	104.5	35.6	21.5	200.3	43.3 ± 12.3	53.6 ± 26.0	85.8 ± 57.4	Q9XT97	PSEN1
22	10050	43.6	51.3	30.0	8.7	7.4	0.6	0.2	10.1	0.1	41.6 ± 6.2[a]	5.6 ± 2.5[b]	3.5 ± 3.3[b]	Q9Y691	KCNMB2
23	14176	54.5	39.8	29.4	152.7	107.6	142.6	0.1	0.1	27.1	41.2 ± 7.3[a]	134.3 ± 13.7[b]	9.1 ± 9.0[a]	Q62273	Slc26a2 Dtd Dtdst
24	7835	37.1	30.8	49.0	31.3	37.7	76.6	14.3	29.7	102.4	39.0 ± 5.3	48.6 ± 14.2	48.8 ± 27.2	Q9Z351	Kcnq2 Kqt2
25	23082	19.2	61.3	33.7	98.5	118.7	458.0	5.5	11.8	108.8	38.1 ± 12.4	225.1 ± 116.6	42.0 ± 33.4	O14863	SLC30A4 ZNT4
26	2390	50.1	43.4	19.0	11.3	20.4	13.9	76.5	46.5	51.1	37.5 ± 9.5[ab]	15.2 ± 2.7[a]	58.0 ± 9.3[b]	Q5ZL05	ORAI1 CRACM1 TMEM142A RCJMB04_8f15
27	15690	72.3	31.1	8.2	64.5	108.8	12.8	8052.8	7545.6	4206.9	37.2 ± 18.8[a]	62.0 ± 27.7[a]	6601.8 ± 1206.4[b]	Q8R2N1	Aqp3
28	18524	39.5	37.3	25.0	8.8	5.1	4.5	47.0	2.2	36.3	34.0 ± 4.5	6.1 ± 1.3	28.5 ± 13.5	Q7RTP0	NIPA1 SPG6
29	16950	22.0	45.5	33.6	201.2	161.9	247.0	0.1	24.1	58.9	33.7 ± 6.8[a]	203.4 ± 24.6[b]	27.7 ± 17.1[a]	Q32KX5	LRRC28
30	306	4.5	95.6	0.2	3.7	35.0	1.7	119.4	74.0	68.2	33.4 ± 31.1	13.5 ± 10.8	87.2 ± 16.2	Q9BQ31	KCNS3

Different alphabet letters indicate statistically significant difference among segments ($P < 0.05$).

Pfaffl, 2006) are recommended. Indeed, consistent PCR amplification of segment-specific marker genes was successfully obtained using the RNA samples excised by LMD from the sections fixed in 1% NBF for 15 min.

In the present study, the five tubular segments (the descending and ascending segments of first and third loops and the collecting tubule) were excised together by LMD. EDT of the third loop, comprised of large columnar cells, is distinguishable from the other four segments within the bundle. Except for EDT, however, morphological characteristics under general staining methods (e.g., HE or PAS) are not sufficient to identify other segments. To identify each segment in the tubular bundle, it is necessary to stain the reference section or the LMD section for marker genes/proteins. The present study confirmed that SGLT2, NKCC2, and UT can be used as specific marker genes/proteins for the ascending segment of first loop, the EDT of third loop, and the collecting tubule, respectively. The formaldehyde-based fixative protocol established in the present study is appropriate for in situ hybridization and immunohistochemistry for improving the LMD protocol in the future.

In the kidney of cloudy catshark, the localization of *sglt2* mRNA signals was confined to the ascending segment of PIa of the first loop. To date, there has been no report showing that the PIa segment is further subdivided into segments with different functions. In the kidney of spiny dogfish, immunoreactive SGLT2 is widely localized in the PIa, PIb, PIIb, LDT, and collecting tubule (Althoff et al., 2006). The observed difference between cloudy catshark and spiny dogfish could be due to methodology, where the former relied on probe specificity for the mRNA and the latter depended on antibody specificity for the protein. The localization of *sglt2* mRNA in the catshark nephron was consistent with that in mammalian nephrons, where SGLT2 is expressed predomi-

Table 3. List of top 30 highly expressed membrane transporter genes in the "2nd" samples.

	GeneID	TPM									Average ± SEM			Accession	Gene name
		2nd_1	2nd_2	2nd_3	4th_1	4th_2	4th_3	B_1	B_2	B_3	2nd	4th	Bundle		
1	**6923**	**1103.1**	**1360.4**	**2624.5**	**162.4**	**38.1**	**102.6**	**7.2**	**4.3**	**20.4**	**1696.0 ± 470.2 [a]**	**101.0 ± 35.9 [b]**	**10.6 ± 5.0 [b]**	**Q8WWT9**	**SLC13A3 NADC3 SDCT2**
2	9560	501.2	744.2	713.5	56.8	21.3	10.1	7.9	3.3	10.2	653.0 ± 76.4 [a]	29.4 ± 14.1 [b]	7.1 ± 2.0 [b]	A1L1P9	slc47a1 mate1 zgc:158231
3	15146	307.0	382.3	1265.3	26.7	14.1	35.9	12.4	6.9	8.2	651.5 ± 307.7	25.6 ± 6.3	9.2 ± 1.6	O75751	SLC22A3 EMTH OCT3
4	7236	331.2	369.9	473.4	21.5	0.9	9.5	19.7	16.7	3.4	391.5 ± 42.4 [a]	10.6 ± 6.0 [b]	13.2 ± 5.0 [b]	Q9Z2J0	Slc23a1 Svct1 Yspl3
5	21113	193.7	377.8	153.8	238.8	117.6	237.0	187.3	307.8	92.3	241.8 ± 69.0	197.8 ± 40.1	195.8 ± 62.4	Q5ZJ06	MAGT1 RCJMB04_22a7
6	22039	183.6	143.8	368.9	9.3	5.1	4.0	0.8	0.2	1.4	232.1 ± 69.4 [a]	6.1 ± 1.6 [b]	0.8 ± 0.4 [b]	Q66J54	slc22a6-a oat1-a
7	15730	255.3	247.9	191.0	71.8	12.5	29.5	76.5	55.0	47.0	231.4 ± 20.3 [a]	37.9 ± 17.6 [b]	59.5 ± 8.8 [b]	A1L2R7	tmem120a
8	23082	98.5	118.7	458.0	5.5	11.8	108.8	19.2	61.3	33.7	225.1 ± 116.6	42.0 ± 33.4	38.1 ± 12.4	O14863	SLC30A4 ZNT4
9	**959**	**52.5**	**115.8**	**479.4**	**1.5**	**0.3**	**2.0**	**2.8**	**1.1**	**3.6**	**215.9 ± 133.0**	**1.3 ± 0.5**	**2.5 ± 0.7**	**Q8N695**	**SLC5A8 AIT SMCT SMCT1**
10	16950	201.2	161.9	247.0	0.1	24.1	58.9	22.0	45.5	33.6	203.4 ± 24.6 [a]	27.7 ± 17.1 [b]	33.7 ± 6.8 [b]	Q32KX5	LRRC28
11	1474	80.3	75.5	404.9	62.0	40.9	392.2	4.5	0.8	4.4	186.9 ± 109.0	165.1 ± 113.8	3.2 ± 1.2	Q0IIV2	rhbg
12	18739	172.9	117.2	260.8	12.9	0.0	4.9	3.2	2.1	3.1	183.6 ± 41.8 [a]	5.9 ± 3.8 [b]	2.8 ± 0.4 [b]	P33527	ABCC1 MRP MRP1
13	2499	111.6	86.3	297.6	0.0	0.0	0.2	6.0	3.4	2.5	165.2 ± 66.6	0.1 ± 0.1	4.0 ± 1.1	Q07837	SLC3A1 RBAT
14	16881	123.8	93.8	216.5	10.1	5.1	8.4	12.5	27.8	16.0	144.7 ± 36.9 [a]	7.9 ± 1.5 [b]	18.8 ± 4.6 [b]	Q6NUT3	MFSD12 C19orf28
15	**15871**	**123.8**	**67.0**	**223.6**	**16.1**	**0.0**	**3.6**	**0.3**	**0.0**	**1.6**	**138.1 ± 45.8 [a]**	**6.6 ± 4.9 [b]**	**0.6 ± 0.5 [b]**	**Q9Z1F2**	**Slc5a11 Kst1 Smit2**
16	7298	115.7	226.2	68.1	25.5	17.4	0.0	7.9	2.3	0.7	136.6 ± 46.8 [a]	14.3 ± 7.5 [b]	3.6 ± 2.2 [b]	Q3T9X0	Slc2a9 Glut9
17	11034	82.0	124.8	198.2	3.2	6.7	2.6	18.1	17.7	19.4	135.0 ± 34.0 [a]	4.2 ± 1.3 [b]	18.4 ± 0.5 [b]	Q62687	Slc6a18 Xtrp2
18	14176	152.7	107.6	142.6	0.1	0.1	27.1	54.5	39.8	29.4	134.3 ± 13.7 [a]	9.1 ± 9.0 [b]	41.2 ± 7.3 [b]	Q62273	Slc26a2 Dtd Dtdst
19	8632	112.3	158.8	90.0	16.4	26.0	43.6	53.3	80.3	17.6	120.3 ± 20.3 [a]	28.7 ± 7.9 [b]	50.4 ± 18.2 [ab]	P82251	SLC7A9 BAT1
20	8550	63.9	110.5	157.0	71.7	42.1	110.7	46.7	121.6	21.9	110.4 ± 26.9	74.8 ± 19.9	63.4 ± 30.0	Q9NRA2	SLC17A5
21	20672	0.0	0.0	267.8	0.0	0.0	0.4	0.0	0.1	19.7	89.3 ± 89.3	0.1 ± 0.1	6.6 ± 6.6	P14222	PRF1 PFP
22	19995	24.1	66.9	149.4	0.1	0.0	26.6	25.2	30.4	8.5	80.1 ± 36.8	8.9 ± 8.8	21.4 ± 6.6	A2A8Z1	Osbpl9 Orp9
23	**5700**	**21.9**	**68.6**	**113.4**	**0.0**	**2.0**	**0.1**	**3.2**	**1.8**	**1.6**	**68.0 ± 26.4 [a]**	**0.7 ± 0.6 [b]**	**2.2 ± 0.5 [ab]**	**O57321**	**SLC1A3 EAAT1**
24	22569	43.1	52.2	106.7	13.8	0.0	23.6	6.1	20.6	11.9	67.3 ± 19.9 [a]	12.5 ± 6.8 [b]	12.9 ± 4.2 [b]	Q9N1R6	SLC7A9 BAT1
25	3374	22.0	61.2	118.0	15.6	0.0	4.2	0.4	0.6	0.5	67.1 ± 27.9	6.6 ± 4.7	0.5 ± 0	P58353	SLC2A5 GLUT5
26	21706	47.7	51.7	93.8	215.9	144.3	250.8	166.9	202.8	690.5	64.4 ± 14.7	203.6 ± 31.3	353.4 ± 168.9	O00299	CLIC1 G6 NCC27
27	7638	31.4	54.2	107.6	41.9	28.6	93.8	34.6	85.6	29.0	64.4 ± 22.6	54.8 ± 19.9	49.7 ± 18.0	P28288	ABCD3 PMP70 PXMP1
28	15690	64.5	108.8	12.8	8052.8	7545.6	4206.9	72.3	31.1	8.2	62.0 ± 27.7 [a]	6601.8 ± 1206.4 [b]	37.2 ± 18.8 [a]	Q8R2N1	Aqp3
29	21430	21.6	26.2	135.7	15.0	0.1	3.5	0.2	0.0	0.0	61.2 ± 37.3	6.2 ± 4.5	0.1 ± 0.1	Q8NG04	SLC26A10
30	19373	6.2	29.4	143.1	1.1	0.0	0.1	5.2	7.4	1.4	59.6 ± 42.3	0.4 ± 0.4	4.7 ± 1.8	Q6UXY8	TMC5 UNQ8238/ PRO33604

Different alphabet letters indicate statistically significant difference among segments ($P < 0.05$). The genes indicated in bold letters with shadow were examined their localization by in situ hybridization.

nantly on the luminal surface of cells of the first part of the proximal tubule (S1 and S2 segments) (Gerich, 2010). The SGLT2 transporter protein is responsible for reabsorbing approximately 90% of the glucose filtered at the glomerulus in mammalian nephrons (see Marsenic, 2009), thus it is reasonable to consider that glucose is predominantly reabsorbed in the early proximal tubules in different vertebrate lineages, including cartilaginous fishes.

Segment-dependent gene expression profiles

In the present study, we successfully obtained lists of genes abundantly expressed in the second loop, fourth loop, and the tubular bundle from the RNA-seq analyses on the LMD samples. We focused on membrane transporter genes, including the slc family, as they play crucial roles in reabsorption and secretion of solutes across the epithelial cells of renal nephrons (Hediger et al., 2004). We found that the marker genes used in the present study were on the lists: *nkcc2*, *sglt2*, and *ut* genes on the "Bundle" list, and *nkcc2* and *ncc* on the "4th" list.

Among the genes on the lists, we further focused on the Na^+-coupled cotransporters abundantly expressed in the second loop because of the following reasons: 1) Na^+-coupled cotransporters are the secondarily active transporters directly contributing to reabsorption or secretion of solutes in nephron segments, and 2) little information has been available on the function of proximal segment(s) in the second loop except possible divalent ion secretion (Hasegawa et al., 2016). The most abundantly expressed slc gene in the second loop was *slc13a3*. In situ hybridization clearly

Table 4. List of top 30 highly expressed membrane transporter genes in the "4th" samples.

	GeneID	TPM									Average ± SEM			Accession	Gene name
		4th_1	4th_2	4th_3	2nd_1	2nd_2	2nd_3	B_1	B_2	B_3	4th	2nd	Bundle		
1	15690	8052.8	7545.6	4206.9	64.5	108.8	12.8	72.3	31.1	8.2	6601.8 ± 1206.4 [a]	62.0 ± 27.7 [b]	37.2 ± 18.8 [b]	Q8R2N1	Aqp3
2	15250	2377.4	1801.0	2514.4	9.4	12.9	10.0	11.7	6.7	7.0	2231.0 ± 218.6 [a]	10.8 ± 1.1 [b]	8.5 ± 1.6 [b]	A9Y006	AQP3
3	20990	356.8	196.0	5062.4	5.0	1.6	8.4	1.6	0.1	3.2	1871.7 ± 1596.0	5.0 ± 2.0	1.6 ± 0.9	H1AFJ6	scnn1b enacbeta
4	22033	1046.1	419.1	2418.8	25.0	26.6	11.4	1953.1	4293.3	1895.5	1294.6 ± 590.5 [ab]	21.0 ± 4.8 [a]	2714.0 ± 789.8 [b]	P55014	Slc12a1 Nkcc2
5	8312	159.5	59.6	859.6	1.3	0.9	2.3	71.9	132.1	55.1	359.6 ± 251.7	1.5 ± 0.4	86.4 ± 23.4	Q9W701	clcnkb
6	15955	165.6	269.2	520.9	0.1	3.9	2.5	42.5	84.6	21.8	318.6 ± 105.5 [a]	2.2 ± 1.1 [b]	49.6 ± 18.5 [b]	O14764	GABRD
7	7120	57.7	55.5	802.3	34.4	12.2	58.9	13.3	62.9	13.0	305.2 ± 248.6	35.2 ± 13.5	29.8 ± 16.6	Q99712	KCNJ15 KCNJ14
8	15691	271.2	413.0	84.0	0.8	6.1	0.1	12.3	12.3	5.6	256.1 ± 95.3 [a]	2.3 ± 1.9 [b]	10.1 ± 2.2 [b]	Q08DE6	AQP3
9	16009	94.5	16.1	538.7	2.0	1.9	1.7	205.7	628.2	169.6	216.4 ± 162.7	1.9 ± 0.1	334.5 ± 147.2	P55016	Slc12a1 Nkcc2
10	21706	215.9	144.3	250.8	47.7	51.7	93.8	166.9	202.8	690.5	203.6 ± 31.3	64.4 ± 14.7	353.4 ± 168.9	O00299	CLIC1 G6 NCC27
11	21113	238.8	117.6	237.0	193.7	377.8	153.8	187.3	307.8	92.3	197.8 ± 40.1	241.8 ± 69.0	195.8 ± 62.4	Q5ZJ06	MAGT1 RCJMB04_22a7
12	1474	62.0	40.9	392.2	80.3	75.5	404.9	4.5	0.8	4.4	165.1 ± 113.8	186.9 ± 109.0	3.2 ± 1.2	Q0IIV2	rhbg
13	12788	84.7	63.7	288.6	9.6	12.4	20.6	9.4	42.8	28.0	145.6 ± 71.7	14.2 ± 3.3	26.7 ± 9.7	Q3MHW6	SLC16A1
14	6923	162.4	38.1	102.6	1103.1	1360.4	2624.5	7.2	4.3	20.4	101.0 ± 35.9 [a]	1696.0 ± 470.2 [b]	10.6 ± 5.0 [a]	Q8WWT9	SLC13A3 NADC3 SDCT2
15	7628	3.4	4.4	287.6	0.5	0.8	0.4	0.6	1.7	0.1	98.5 ± 94.6	0.6 ± 0.1	0.8 ± 0.5	P55017	SLC12A3 NCC TSC
16	22145	4.0	11.6	258.0	0.0	0.0	0.1	0.0	0.0	5.2	91.2 ± 83.4	0 ± 0	1.7 ± 1.7	K7GET2	SCNN1A
17	306	119.4	74.0	68.2	3.7	35.0	1.7	4.5	95.6	0.2	87.2 ± 16.2	13.5 ± 10.8	33.4 ± 31.1	Q9BQ31	KCNS3
18	14778	35.6	21.5	200.3	18.6	37.9	104.5	25.6	66.9	37.5	85.8 ± 57.4	53.6 ± 26.0	43.3 ± 12.3	Q9XT97	PSEN1
19	8888	67.6	78.0	88.0	25.8	62.6	56.3	66.3	210.2	45.4	77.9 ± 5.9	48.2 ± 11.4	107.3 ± 51.8	Q8N8Q9	NIPA2
20	8550	71.7	42.1	110.7	63.9	110.5	157.0	46.7	121.6	21.9	74.8 ± 19.9	110.4 ± 26.9	63.4 ± 30.0	Q9NRA2	SLC17A5
21	2390	76.5	46.5	51.1	11.3	20.4	13.9	50.1	43.4	19.0	58.0 ± 9.3 [a]	15.2 ± 2.7 [b]	37.5 ± 9.5 [ab]	Q5ZL05	ORAI1 CRACM1 TMEM142A RCJMB04_8f15
22	6217	85.2	63.0	23.8	15.9	7.0	73.5	41.7	77.2	64.7	57.3 ± 18.0	32.1 ± 20.8	61.2 ± 10.4	A8WHP3	slc5a9 si:dkey-7o6.5
23	6841	33.3	9.3	124.5	0.0	0.3	0.3	0.2	1.0	0.1	55.7 ± 35.1	0.2 ± 0.1	0.4 ± 0.3	Q8NBS3	SLC4A11 BTR1
24	7638	41.9	28.6	93.8	31.4	54.2	107.6	34.6	85.6	29.0	54.8 ± 19.9	64.4 ± 22.6	49.7 ± 18.0	P28288	ABCD3 PMP70 PXMP1
25	7835	14.3	29.7	102.4	31.3	37.7	76.6	37.1	30.8	49.0	48.8 ± 27.2	48.6 ± 14.2	39.0 ± 5.3	Q9Z351	Kcnq2 Kqt2
26	6469	17.3	5.7	123.1	9.4	18.1	43.3	15.9	32.6	23.2	48.7 ± 37.3	23.6 ± 10.2	23.9 ± 4.8	Q6GPA5	ttyh3
27	14266	6.6	16.8	113.5	0.0	4.2	16.1	11.5	21.3	15.4	45.6 ± 34.1	6.8 ± 4.8	16.1 ± 2.8	Q4R6K2	SLC30A1 ZNT1 QtsA-11880 QtsA-17815
28	17857	0.4	7.0	120.3	2.8	11.3	62.6	10.3	32.5	6.5	42.6 ± 38.9	25.6 ± 18.7	16.4 ± 8.1	Q4GZT3	PKD2 TRPP2
29	9331	3.2	0.3	124.0	25.7	17.6	93.7	3.0	9.4	0.6	42.5 ± 40.8	45.7 ± 24.1	4.3 ± 2.6	O60346	PHLPP1 KIAA0606 PHLPP PLEKHE1 SCOP
30	23082	5.5	11.8	108.8	98.5	118.7	458.0	19.2	61.3	33.7	42.0 ± 33.4	225.1 ± 116.6	38.1 ± 12.4	O14863	SLC30A4 ZNT4

Different alphabet letters indicate statistically significant difference among segments ($P < 0.05$).

showed that *slc13a3* mRNA is abundantly expressed in the PII segment of the second loop. The Slc13 family is comprised of five members that encode electrogenic Na^+-coupled cotransporters for anions or di- and tri-carboxylates (Markovich and Murer, 2004). In mammalian kidneys, Slc13a3 is localized on the basolateral membrane of the proximal tubule, and transport intermediates of the Krebs cycle such as succinate, citrate, and α-ketoglutarate (Bergeron et al., 2013). Slc13a3 also plays an important role in the renal elimination of xenobiotics by secreting organic anions into urine.

The renal secretion of organic anions is considered to be achieved with several steps as follows (Breljac et al., 2016): 1) primary active NKA creates an inwardly directed Na^+ gradient, 2) secondary active Na^+-coupled dicarboxylate cotransporter (Slc13a3) creates an outwardly directed gradient of α-ketoglutarate, and 3) tertiary active organic anion transporters (such as Slc22a6 and Slc22a8) transport organic anions into epithelial cells by exchanging organic anions with α-ketoglutarate. All three components (NKA, Slc13a3, and Slc22a6 or Slc22a8) were localized on the basolateral membrane (see Breljac et al., 2016). On the apical membrane, 4) multiple ATP-binding cassette (ABC) and Slc transporters secrete organic anions into the lumen of the proximal tubule (Schlatter et al., 2006). In this regard, our RNA-seq data supported such a scheme for the shark nephron since the transcripts of *slc22a6* and *abcc1* genes were on the list of highly expressed membrane transporter genes in the second loop. These results suggest that the PII segment of the second loop contributes to secretion of organic

anions in the elasmobranch nephron, in addition to divalent ion secretion.

In the list of highly expressed transporters in the second loop, two Slc5 members were found, *slc5a8* and *slc5a11*. The *slc5a11* mRNA was localized in the PII segment of the second loop, while *slc5a8* mRNA signals were co-localized with *sglt2* mRNA in the ascending part of the PIa segment in the bundle zone (Figure 4). The Slc5 family is known as the Na^+-coupled glucose cotransporter family, but these proteins also transport monocarboxylates such as lactate and pyruvate, short-chain fatty acids, and ketone bodies (Plata et al., 2007). Slc5a8 transports monocarboxylates and ketone bodies, and thus was named Na^+-coupled monocarboxylate transporter (SMCT1) (Gopal et al., 2004). In mammalian kidneys, the reabsorption fraction of lactate from the glomerular filtrate is over 95%. In the renal tubular system, lactate and ketone bodies are also used as the major fuels for active reabsorption of electrolytes and nutrients (Yanase et al., 2008). Since an increased reliance on ketone bodies as an energy source was observed following prolonged starvation in elasmobranchs (Zammit and Newsholme, 1979), Slc5a8 could have a regulatory role in energy metabolism in the elasmobranch nephron. Since both *sglt2* and *slc5a8* mRNAs were expressed in the ascending part of PIa segment, it is likely that this segment is important for reabsorption of energy substrates such as glucose, lactate, and ketone bodies. On the other hand, Slc5a11 (SGLT6) is a Na^+-coupled myo-inositol cotransporter in the apical membrane of renal tubule cells, where it mediates myo-inositol reabsorption from the primary urine (Kottgen et al., 2018). Myo-inositol and its derivatives have functions including regulation of ion channels, metabolic flux, mRNA transcription and translation, stress response, and embryonic development (Kiani et al., 2021). In the kidney, myo-inositol is also important as a protective osmolyte against osmotic stress.

slc1a3, which is another slc gene examined in the present study, is a member of glutamate/neutral amino acid transporters. The TPM value of *slc1a3* was less than 5% of that of *slc13a3*, and we could not confirm the gene expression site by in situ hybridization due to the low expression level. Slc1a3 is a glial-type glutamate transporter (also known as a glutamate-aspartate transporter, GLAST, or an excitatory amino acid transporter, EAAT1) abundantly expressed in the cerebellum in mammals (Kanai and Hediger, 2004). Slc1a3 is responsible for glutamate uptake in the brain, which is crucial for glutamatergic neurotransmission by removing glutamate from the synaptic cleft (Berger and Hediger, 2006). However, expression of the *Slc1a3* gene has not been proven in mammalian renal tubules. Instead, another glutamate transporter, Slc1a1, is localized in the apical membrane of proximal tubules in the mammalian kidneys (Berger and Hediger, 2006). *Slc1a1*-knockout mice exhibited dicarboxylic aminoaciduria, confirming its crucial role for reabsorbing glutamate in the proximal tubule (Kanai and Hediger, 2004). Further investigations on *slc1a1* and *slc1a3* mRNAs are required to understand their roles in the kidney of elasmobranchs.

Seawater is an environment of excess divalent ions, and thus the kidneys of marine teleosts and cartilaginous fishes must excrete divalent ions. Excretion of NaCl is achieved by the branchial ionocytes (teleost fishes) and the rectal gland (cartilaginous fishes), whereas it has been well documented that kidneys are responsible for the excretion of divalent ions (see Takvam et al., 2021). We previously revealed co-localization of sulfate transporters Slc26a1 and Slc26a6 in the basolateral and apical membranes, respectively, in the PII segment of the elephant fish nephron, implying that the PII segment of the second loop is a secretory segment for excess solutes (Hasegawa et al., 2016). In the present study, we found intense expression of *slc13a3* mRNA in the PII segment. As mentioned above, Slc13a3 most likely contributes to the renal elimination of xenobiotics by secreting organic anions into urine, further supporting the secretory role of the PII segment. On the other hand, expression of Na^+-coupled myo-inositol transporter (*slc5a11*) mRNA was also found in the PII segment. Although the cellular localization of Slc5a11 is uncertain in the cartilaginous fish nephron, distribution of these transporters in the apical membrane has been well documented in the mammalian nephron. These results imply that the PII segment may not be a simple secretory segment, but it may also be involved in reabsorption of valuable solutes. In the catshark nephron, at least four segments can be identified in the proximal tubule: the descending PIa (the first loop with no expression of *sglt2* mRNA), the ascending PIa (the first loop with *sglt2* and *slc5a8* mRNAs), PIb, and PII (with *slc13a3* and *slc5a11* mRNAs). To understand further the function of each segment, finer-scale clipping of each segment by the LMD is required, with the guidance of reference section stained with in situ hybridization and/or immunohistochemistry.

Among the four slc transporters examined in the second loop, expressions of *slc5a11* and *slc13a3* were only detected in the PII segment by in situ hybridization, confirming the quantitative results of RNA-seq from the LMD samples. However, expression of *slc5a8* mRNA was detected in the ascending part of PIa segment in the bundle zone, which is inconsistent with the low TPM values of *slc5a8* in the "Bundle" samples (4.4 ± 1.0). Since the TPM values of *sglt2* (*slc5a2*) that marked the PIa segment were significantly high in the "Bundle" samples, it is uncertain why the TPM values of *slc5a8* mRNA were low in the "Bundle" samples. Perhaps unannotated contig(s) encoding *Slc5a8* exists in the RNA-seq data of the "Bundle" samples, leading to incomplete counting of transcripts.

Conclusion and perspectives

In the present study, we developed a protocol for clipping specific nephron segments of catshark kidney by LMD, and successfully conducted subsequent RNA-seq analysis for profiling the segment-dependent gene expressions. Most cartilaginous fishes are obligatory marine species, while a limited number of sharks and rays have the ability to inhabit low salinity environments (Ballantyne and Robinson, 2010). During the acclimation to low salinity environments, euryhaline sharks and rays produce large volumes of dilute urine to excrete excess water; they do this by increasing glomerular filtration and solute reabsorption in the renal tubules (Janech et al., 2006; Imaseki et al., 2019; Aburatani et al., 2022). Indeed, we found marked increase in the expression of the *ncc* gene in the LDT of FW-acclimated bull shark, *Carcharhinus leucas* (Imaseki et al., 2019), and of the *nkcc2* gene in the EDT of FW-acclimated red stingray, *Hemitrygon*

akajei (Aburatani et al., 2020). It is likely that water reabsorption in renal tubules would also be decreased in low salinity environments. Currently, regulatory mechanisms of renal function remain poorly resolved in euryhaline elasmobranchs, and therefore, the segment-dependent gene expression profiling that we report here will be a powerful technique for unraveling the renal mechanisms and regulation in euryhaline elasmobranchs.

ACKNOWLEDGMENTS

We are grateful to Ms. Kiriko Ikeba and Dr. Taro Watanabe of AORI for help with keeping the animals, and Ms. Sugako Watanabe and Mr. Koya Shimoyama of AORI for preparing illustrations and figures. We are grateful to Prof. Christopher A. Loretz of the State University of New York at Buffalo for his critical reading of this manuscript. This study was supported by Grants-in-Aid for Scientific Research from the Japan Society for the Promotion of Science to SH (JSPS KAKENHI 17H03868 and 19K22414) and to WT (JSPS KAKENHI 22K15153), and a Grant-in-Aid for JSPS Fellows to NA (21J20882). NA is supported by JSPS Research Fellowships for Young Scientists.

COMPETING INTERESTS

The authors have no competing interests to declare.

AUTHOR CONTRIBUTIONS

TH and SH designed the study. TH, WT, NA, MY, MI, and MT performed the experiments and collected data. TH, WT, NA, and KT kept the animals and contributed to sample collection. WT, MI, KO, RO-K, and MK-SW supervised the experiments. TH and SH wrote the first draft of the manuscript, and WT, NA, MK-SW, and SH largely contributed to the revision step. All of the authors contributed substantial input to the final version of the manuscript.

SUPPLEMENTARY MATERIALS

Supplementary material for this article is available online. (URL: https://doi.org/10.2108/zs220092)

Supplementary Table S1. Primer sets used for quantitative PCR and in situ hybridization.

REFERENCES

Aburatani N, Takagi W, Wong MKS, Kadota M, Kuraku S, Tokunaga K, et al. (2020) Facilitated NaCl uptake in the highly developed bundle of the nephron in Japanese red stingray *Hemitrygon akajei* revealed by comparative anatomy and molecular mapping. Zool Sci 37: 458–466

Aburatani N, Takagi W, Wong MKS, Kuraku S, Tanegashima C, Kadota M, et al. (2022) Molecular and morphological investigations on the renal mechanisms enabling euryhalinity of red stingray *Hemitrygon akajei*. Front Physiol 13: 953665

Althoff T, Hentschel H, Luig J, Schutz H, Kasch M, Kinne RKH (2006) Na^+-D-glucose cotransporter in the kidney of *Squalus acanthias*: molecular identification and intrarenal distribution. Am J Physiol Regul Integr Physiol 290: R1094–R1104

Anderson WG, Taylor JR, Good JP, Hazon N, Grosell M (2007) Body fluid volume regulation in elasmobranch fish. Comp Biochem Physiol A 148: 3–13

Auerbach C, Moutschen-Dahmen M, Moutschen J (1977) Genetic and cytogenetical effects of formaldehyde and related compounds. Mutat Res 39: 317–362

Ballantyne JS, Robinson JW (2010) Freshwater elasmobranchs: a review of their physiology and biochemistry. J Comp Physiol B 180: 475–493

Berger UV, Hediger MA (2006) Distribution of the glutamate transporters GLT-1 (SLC1A2) and GLAST (SLC1A3) in peripheral organs. Anat Embryol 211: 595–606

Bergeron MJ, Clemencon B, Hediger MA, Markovich D (2013) SLC13 family of Na^+-coupled di- and tri-carboxylate/sulfate transporters. Mol Aspects Med 34: 299–312

Boylan JW (1967) Gill permeability in *Squalus acanthias*. In "Sharks, Skates and Rays" Ed by PW Gilbert, RF Mathewson, DP Rall, Johns Hopkins Press, Baltimore, pp 197–206

Breljak D, Ljubojevic MI, Hagos Y, Micek V, Eror DB, Madunic IV, et al. (2016) Distribution of organic anion transporters NaDC3 and OAT1-3 along the human nephron. Am J Physiol Renal Physiol 311: F227–F238

Chung JY, Braunschweig T, Williams R, Guerrero N, Hoffmann KM, Kwon M, et al. (2008) Factors in tissue handling and processing that impact RNA obtained from formalin-fixed, paraffin-embedded tissue. J Histochem Cytochem 56: 1033–1042

Dobin A, Davis CA, Schlesinger F, Drenkow J, Zaleski C, Jha S, et al. (2013) STAR: ultrafast universal RNA-seq aligner. Bioinformatics 29: 15–21

Espina V, Wulfkuhle JD, Calvert VS, VanMeter A, Zhou W, Coukos G, et al. (2006) Laser-capture microdissection. Nat Protoc 1: 586–603

Fleige S, Pfaffl MW (2006) RNA integrity and the effect on the real-time qRT-PCR performance. Mol Aspects Med 27: 126–139

Gerich JE (2010) Role of the kidney in normal glucose homeostasis and in the hyperglycaemia of diabetes mellitus: therapeutic implications. Diabet Med 27: 136–142

Goldstein L, Forster RP (1971) Osmoregulation and urea metabolism in the little skate *Raja erinacea*. Am J Physiol 224: 367–372

Gopal E, Fei YJ, Sugawara M, Miyauchi S, Zhuang L, Martin P, et al. (2004) Expression of *slc5a8* in kidney and its role in Na^+-coupled transport of lactate. J Biol Chem 279: 44522–44532

Hara Y, Yamaguchi K, Onimaru K, Kadota M, Koyanagi M, Keeley SD, et al. (2018) Shark genomes provide insights into elasmobranch evolution and the origin of vertebrates. Nat Ecol Evol 2: 1761–1771

Hasegawa K, Kato A, Watanabe T, Takagi W, Romero MF, Bell JD, et al. (2016) Sulfate transporters involved in sulfate secretion in the kidney are localized in the renal proximal tubule II of the elephant fish (*Callorhinchus milii*). Am J Physiol 311: R66–R78

Hazon N, Wells A, Pillans RD, Good JP, Anderson WG, Franklin CE (2003) Urea based osmoregulation and endocrine control in elasmobranch fish with special reference to euryhalinity. Comp Biochem Physiol B 136: 685–700

Hediger MA, Romero MF, Peng JB, Rolfs A, Takanaga H, Bruford EA (2004) The ABCs of solute carriers: physiological, pathological and therapeutic implications of human membrane transport proteins. Eur J Physiol 447: 465–468

Hentschel H (1987) Renal architecture of the dogfish *Scyliorhinus caniculus* (Chondrichthyes, Elasmobranchii). Zoomorphology 107: 115–125

Hentschel H, Mähler S, Herter P, Elger M (1993) Renal tubule of dogfish, *Scyliorhinus caniculus*: A comprehensive study of structure with emphasis on intramembrane particles and immunoreactivity for H^+-K^+-adenosine triphosphatase. Anat Rec 235: 511–532

Hyodo S, Katoh F, Kaneko T, Takei Y (2004) A facilitative urea transporter is localized in the renal collecting tubule of the dogfish *Triakis scyllia*. J Exp Biol 207: 347–356

Hyodo S, Kakumura K, Takagi W, Hasegawa K, Yamaguchi Y (2014) Morphological and functional characteristics of the kidney of cartilaginous fishes: with special reference to urea reabsorption. Am J Physiol 307: R1381–R1395

Imaseki I, Wakabayashi M, Hara Y, Watanabe T, Takabe S, Kakumura K, et al. (2019) Comprehensive analysis of genes contributing to euryhalinity in the bull shark, *Carcharhinus leucas*; Na^+-Cl^- co-transporter is one of the key renal factors

upregulated in acclimation to low-salinity environment. J Exp Biol 222: jeb201780
Janech MG, Fitzgibbon WR, Ploth DW, Lacy ER, Miller DH (2006) Effect of low environmental salinity on plasma composition and renal function of the Atlantic stingray, a euryhaline elasmobranch. Am J Physiol 291: F770–F780
Kakumura K, Takabe S, Takagi W, Hasegawa K, Konno N, Bell JD, et al. (2015) Morphological and molecular investigations of the holocephalan elephant fish nephron: the existence of a countercurrent-like configuration and two separate diluting segments in the distal tubule. Cell Tissue Res 362: 677–688
Kanai Y, Hediger MA (2004) The glutamate/neutral amino acid transporter family SLC1: molecular, physiological and pharmacological aspects. Eur J Physiol 447: 469–479
Kempton R (1953) Studies on the elasmobranch kidney-II. Reabsorption of urea by smooth dogfish, *Mustelus canis*. Biol Bull 104: 45–56
Kiani AK, Paolacci S, Calogero AE, Cannarella R, Di Renzo GC, Gerli S, et al. (2021) From Myo-inositol to D-chiro-inositol molecular pathways. Eur Rev Med Pharmacol Sci 25: 2390–2402
Kottgen A, Raffler J, Sekula P, Kastenmuller G (2018) Genome-wide association studies of metabolite concentrations (mGWAS): relevance for nephrology. Semin Nephrol 38: 151–174
Lacy ER, Reale E (1985a) The elasmobranch kidney. I. Gross anatomy and general distribution of the nephrons. Anat Embryol 173: 23–24
Lacy ER, Reale E (1985b) The elasmobranch kidney. II. Sequence and structure of the nephrons. Anat Embryol 173: 163–186
Liao Y, Smyth GK, Shi W (2014) FeatureCounts: an efficient general purpose program for assigning sequence reads to genomic features. Bioinformatics 30: 923–930
Lykidis D, Van Noorden S, Armstrong A, Spencer-Dene B, Li J, Zhuang Z, et al. (2007) Novel zinc-based fixative for high quality DNA, RNA and protein analysis. Nucleic Acids Res 35: e85
Madsen SS, Bollinger RJ, Brauckhoff M, Engelund MB (2020) Gene expression profiling of proximal and distal renal tubules in Atlantic salmon (*Salmo salar*) acclimated to fresh water and seawater. Am J Physiol Renal Physiol 319: F380–F393
Markovich D, Murer H (2004) The SLC13 gene family of sodium sulphate/carboxylate cotransporters. Eur J Physiol 447: 594–602
Marsenic O (2009) Glucose control by the kidney: an emerging target in diabetes. Am J Kid Dis 53: 875–883
Masuda N, Ohnishi T, Kawamoto S, Monden M, Okubo K (1999) Analysis of chemical modification of RNA from formalin-fixed samples and optimization of molecular biology applications for such samples. Nucleic Acids Res 27: 4436–4443
Murray GI (2007) An overview of laser microdissection technologies. Acta Histochem 109: 171–176
Pang PK, Griffith RW, Atz JW (1977) Osmoregulation in elasmobranchs. Am Zool 17: 365–377
Park YN, Abe K, Li H, Hsuih T, Thung SN, Zhang DY (1996) Detection of hepatitis C virus RNA using ligation-dependent polymerase chain reaction in formalin-fixed, paraffin-embedded liver tissues. Am J Pathol 149: 1485–1491
Payan P, Goldstein L, Forster RP (1973) Gills and kidneys in ureosmotic regulation in euryhaline skates. Am J Physiol 224: 367–372
Plata C, Sussman CR, Sindic A, Liang JO, Mount DB, Josephs ZM, et al. (2007) Zebrafish Slc5a12 encodes an electroneutral sodium monocarboxylate transporter (SMCTn). J Biol Chem 282: 11996–12009
Puchtler H, Waldrop FS, Meloan SN, Terry MS, Conner HM (1970) Methacarn (methanol-Carnoy) fixation. Histochemie 21: 97–116
Romero IG, Pai AA, Tung J, Gilad Y (2014) RNA-seq: impact of RNA degradation on transcript quantification. BMC Biol 12: 42
Sasagawa Y, Nikaido I, Hayashi T, Danno H, Uno KD, Imai T, Ueda HR (2013) Quartz-Seq: a highly reproducible and sensitive single-cell RNA sequencing method, reveals non-genetic gene-expression heterogeneity. Genome Biol 14: R31
Schlatter P, Gutmann H, Drewe J (2006) Primary porcine proximal tubular cells as a model for transepithelial drug transport in human kidney. Eur J Pharm Sci 28: 141–154
Schroeder A, Mueller O, Stocker S, Salowsky R, Leiber M, Gassmann M, et al. (2006) The RIN: an RNA integrity number for assigning integrity values to RNA measurements. BMC Mol Biol 7: 3
Smith HW (1936) The retention and physiological role of urea in the elasmobranchii. Biol Rev 11: 49–82
Takabe S, Teranishi K, Takaki S, Kusakabe M, Hirose S, Kaneko T, Hyodo S (2012) Morphological and functional characterization of a novel Na^+/K^+-ATPase-immunoreactive, follicle-like structure on the gill septum of Japanese banded houndshark, *Triakis scyllium*. Cell Tissue Res 348: 141–153
Takagi W, Kajimura M, Tanaka H, Hasegawa K, Ogawa S, Hyodo S (2017) Distributional shift of urea production site from the extra-embryonic yolk sac membrane to the embryonic liver during the development of cloudy catshark (*Scyliorhinus torazame*). Comp Biochem Physiol A 211: 7–16
Takvam M, Wood CM, Kryvi H, Nilsen TO (2021) Ion transporters and osmoregulation in the kidney of teleost fishes as a function of salinity. Front Physiol 12: 664588
Vincek V, Nassiri M, Nadji M, Morales AR (2003) A tissue fixative that protects macromolecules (DNA, RNA, and protein) and histomorphology in clinical samples. Lab Invest 83: 1427–1435
Yanase H, Takebe K, Nio-Kobayashi J, Takahashi-Iwanaga H, Iwanaga T (2008) Cellular expression of a sodium-dependent monocarboxylate transporter (Slc5a8) and the MCT family in the mouse kidney. Histochem Cell Biol 130: 957–966
Zammit VA, Newsholme EA (1979) Activities of enzymes of fat and ketone-body metabolism and effects of starvation on blood concentrations of glucose and fat fuels in teleost and elasmobranch fish. Biochem J 184: 313–322

(Received October 18, 2022 / Accepted November 21, 2022 / Published online January 18, 2023)